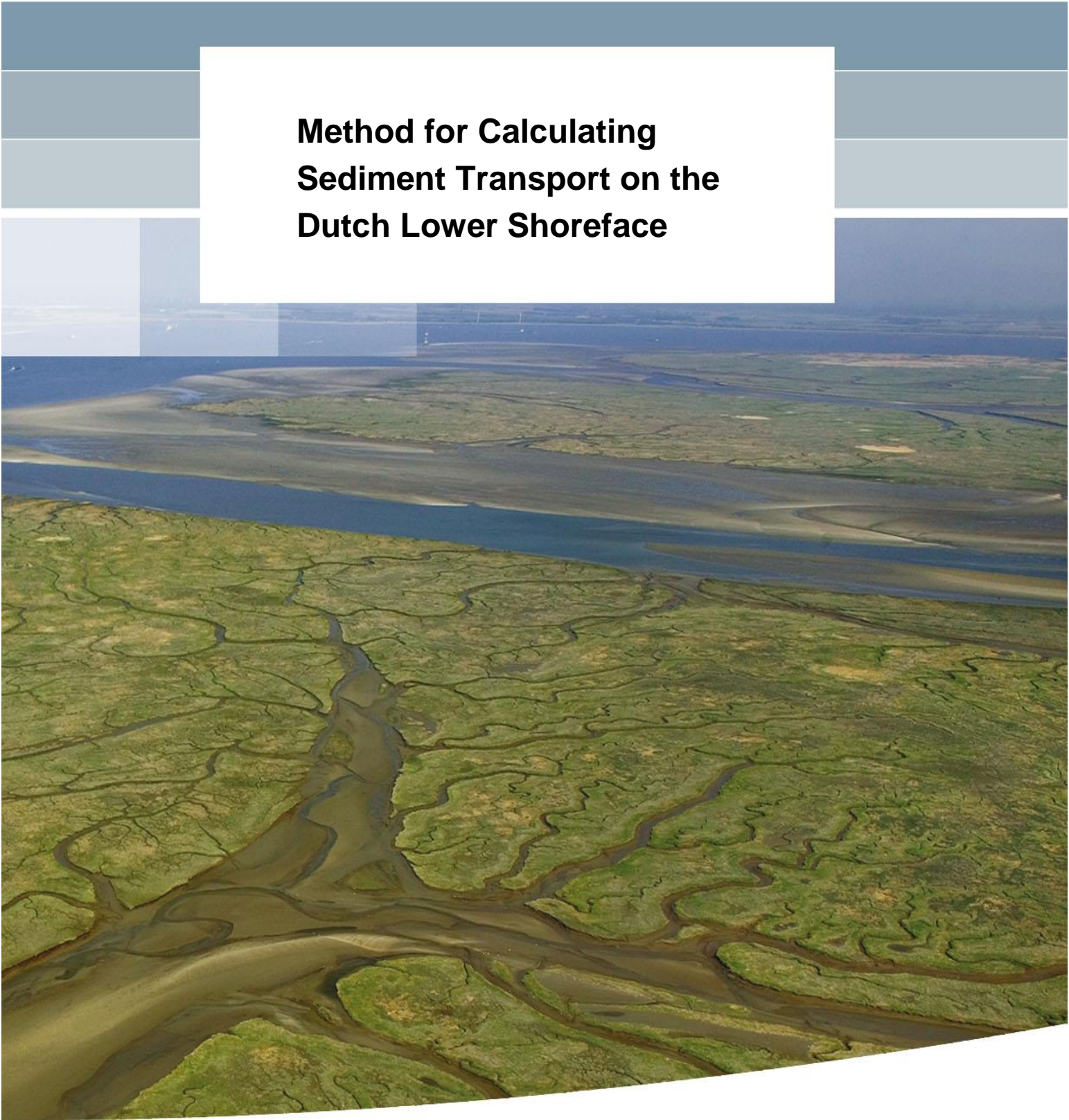


**Method for Calculating
Sediment Transport on the
Dutch Lower Shoreface**



Method for Calculating Sediment Transport on the Dutch Lower Shoreface

Bart Grasmeijer

1220339-000

Title

Method for Calculating Sediment Transport on the Dutch Lower Shoreface

Client	Project	Reference	Pages
Rijkswaterstaat	1220339-000	1220339-000-ZKS-0041	25

Keywords

Coastal Genesis, Sediment Transport, Coastal Foundation, Dutch Lower Shoreface Morphodynamics, Numerical Modelling

Summary

This report describes an offline Sediment Transport Model for the Dutch Lower Shoreface that can compute annual sand transport rates at arbitrary locations along the lower shoreface of the Dutch coast. The approach is based on output of the state-of-the-art 3D DCSM-FM model, wave observations together with a wave transformation matrix for the Dutch coast and a 1DV sand transport module.




The average annual alongshore transport rates computed here at the Noordwijk transect encouragingly agree with the bandwidth presented by Van Rijn (1997) for the same transect.

The average annual cross-shore transport rates computed here agree with estimates by Hop (2017) and Waagmeester (2015) at the Noordwijk transect using the Soulsby-Van Rijn transport formulation but are smaller than the best estimate presented by Van Rijn (1997).

The variation in annual transports is relatively large per year (~40-50%).

The effect of a larger D_{50} is relatively small (~10%) compared to the variation per year.

In the next phase of the project the model will be validated with an online approach. The model results will also be compared with flow, wave and transport measurements made at the lower shoreface of Ameland, Terschelling and Noordwijk.

Version	Date	Author	Initials	Review	Initials	Approval	Initials
0.3	4 May 2018	Bart Grasmeijer		Arjen Luijendijk		Frank Hoozemans	
0.4	2 July 2018	Bart Grasmeijer		Arjen Luijendijk		Frank Hoozemans	
0.5	11 July 2018	Bart Grasmeijer		Arjen Luijendijk		Frank Hoozemans	

State
final

Content

1 Introduction	1
1.1 Background	1
1.2 Objective and scope	1
1.3 Outline of the report	1
2 Dutch shoreface and coastal foundation	3
2.1 Dutch shoreface	3
2.2 Coastal foundation	4
3 Methods to calculate transport at shoreface	7
3.1 3D Dutch Continental Shelf Model-Flexible Mesh (3D DCSM-FM)	7
3.2 Wave transformation matrix	8
3.3 Sediment transport model	9
3.3.1 Suspended sand transport	9
3.3.2 Bedload sand transport	10
3.3.3 Total load transport	11
4 Validation of method at Noordwijk	13
4.1 Flow and salinity	13
4.2 Waves	15
4.3 Annual transports rates	16
4.3.1 Alongshore transport rates	18
4.3.2 Cross-shore transport rates	18
5 Discussion, conclusions and recommendations	21
5.1 Discussion	21
5.2 Conclusions	23
5.3 Next steps	23
References	25
Appendices	
A TSAND model	A-1
B Wave transformation matrix	B-1
C Wave time series for NOORDWK20	C-1
D Joint occurrence tables wave height and direction for NOORDWK20	D-1

1 Introduction

1.1 Background

Dutch coastal policy aims for a safe, economically strong and attractive coast. This is achieved by maintaining the part of the coast that support these functions; the coastal foundation. The coastal foundation is maintained by means of sand nourishments; the total nourishment volume is approximately 12 million m³/year since 2000.

In 2020 the Dutch Ministry of Infrastructure and Environment will make a decision on the nourishment volume. The Kustgenese-2 (KG2) programme is aimed to deliver knowledge to enable this decision making. The scope of the KG2 project commissioned by Rijkswaterstaat to Deltares is determined by two main questions:

- 1 What are possibilities for an alternative offshore boundary of the coastal foundation?
- 2 How much sediment is required for the coastal foundation to grow with sea level rise?

The Deltares KG2 subproject “Diepere Vooroever” (DV, lower shoreface), of which this report is a small part, answers both questions. The KG2-DV project will study the sediment transports of the Dutch lower shoreface, in particular the net cross-shore sand transport as function of depth on the basis of field measurements, numerical modelling and system knowledge.

1.2 Objective and scope

The study focusses on the Dutch lower shoreface which is defined as the area between the upper shoreface (with regular and dominant wave action) and the shelf (no serious wave action). This is roughly the zone between the outer breaker bar (approx. NAP -8 m) and the NAP -20 m depth contour. The latter has been defined as the offshore boundary of the coastal foundation (Lodder, 2016).

This report presents a so-called offline method to compute the sediment transport rates on the Dutch lower shoreface and presents initial results. The approach is called offline because tide and wind-driven flow velocities are computed independently of waves first and waves are also assessed independently of flow. Flow and waves are combined thereafter to compute the sediment transports. In this offline approach, the waves do not interact with the flow, thus ignoring effects waves may have on the velocity profile. In contrast, in an online approach, current and wave computations are coupled where waves may affect the flow profile and vice versa.

The purpose of this report is to investigate the feasibility and skill of the offline approach. In a later phase, comparisons will be made with KG2 measurements and the impact of an online approach on the annual sediment transport rates will be investigated.

The final purpose of the sediment transport computations is to assess the annual sediment transport rates across the present offshore boundary at -20 m. Furthermore, this approach could be applied in case an alternative offshore boundary of the coastal foundation will be considered (beyond the present scope).

1.3 Outline of the report

This report is organised as follows. Chapter 2 defines the Dutch shoreface and coastal foundation. Chapter 3 describes the method applied to determine the cross-shore transport rates. Chapter 4 presents the preliminary results while chapter 5 presents the discussion, conclusions and recommendations.

2 Dutch shoreface and coastal foundation

2.1 Dutch shoreface

The shoreface is the active littoral zone between the low water line and the continental shelf. As different shoreface subzone classifications (see e.g. Van Rijn (1998)) exist, we first summarize our definitions. The upper shoreface is here defined as the surf zone between the waterline and approximately the NAP -8 m depth contour. Typical bed slopes are found varying between 1:50 to 1:200 (Figure 2.1). We define the lower shoreface as the zone between approx. the NAP -8 m and NAP -20 m depth contours with typical bed slopes between 1:200 and 1:1000, and where sand ridges may be present¹. Beyond the NAP -20 m, the shoreface merges with the continental shelf where the slope is generally gentler than 1:1000; tidal sand waves and sand banks may be present here.

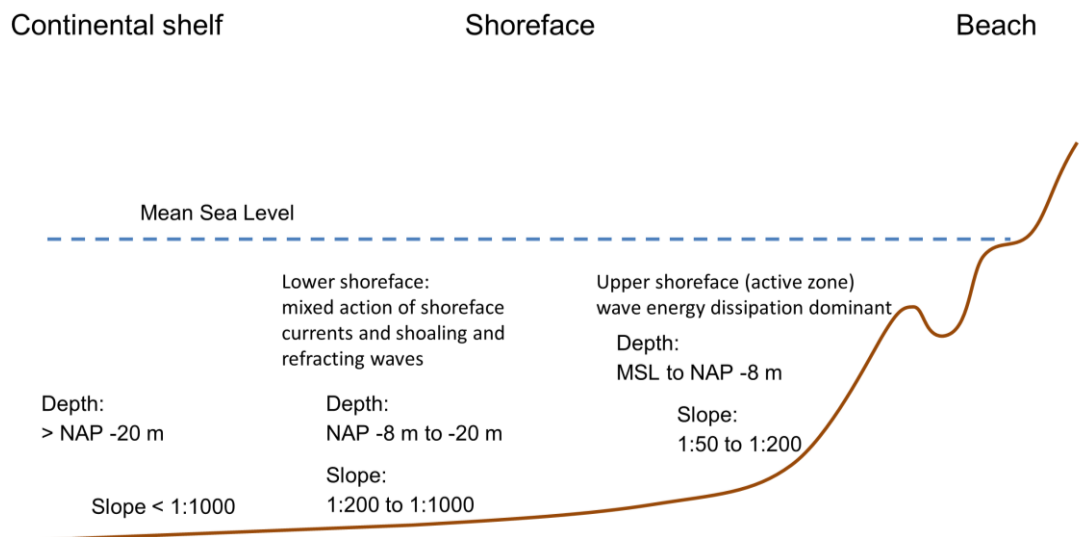


Figure 2.1 Typical Dutch cross-shore coastal profile (not to vertical scale).

The effects due to wave energy dissipation are dominant in the upper shoreface. The upper shoreface is denoted as “active zone” as transport rates are relatively large and the morphological response time is short, almost on the scale of events. The lower shoreface is the zone where the mixed action of shoreface currents (incl. tide) and shoaling and refracting waves is predominant. Transport rates are relatively small and hence the bed levels in the lower shoreface undergo relatively slow adaptations.

The shape of the shoreface profile differs along the Dutch coast. For instance, the shoreface profile along tidal deltas has a convex shape, while the shoreface profile along the Holland coast has a concave shape. For more information, we refer to the literature review by Van der Werf et al. (2017), who discuss the Dutch shoreface morphology and underlying physical processes.

The Dutch shoreface morphology and underlying physical processes are further discussed by Van der Werf et al (2017).

¹ Van Rijn (1998) calls this the middle shoreface.

2.2 Coastal foundation

Dutch coastal policy aims for a safe, economically strong and attractive coast. This is achieved by maintaining the part of the coast that supports these functions; the coastal foundation. The offshore boundary of the coastal foundation is taken at the NAP -20 m depth contour; the onshore limit is formed by the landward edge of the dune area (closed coast) and by the tidal inlets (open coast). The borders with Belgium and Germany are the lateral boundaries (Figure 2.2).

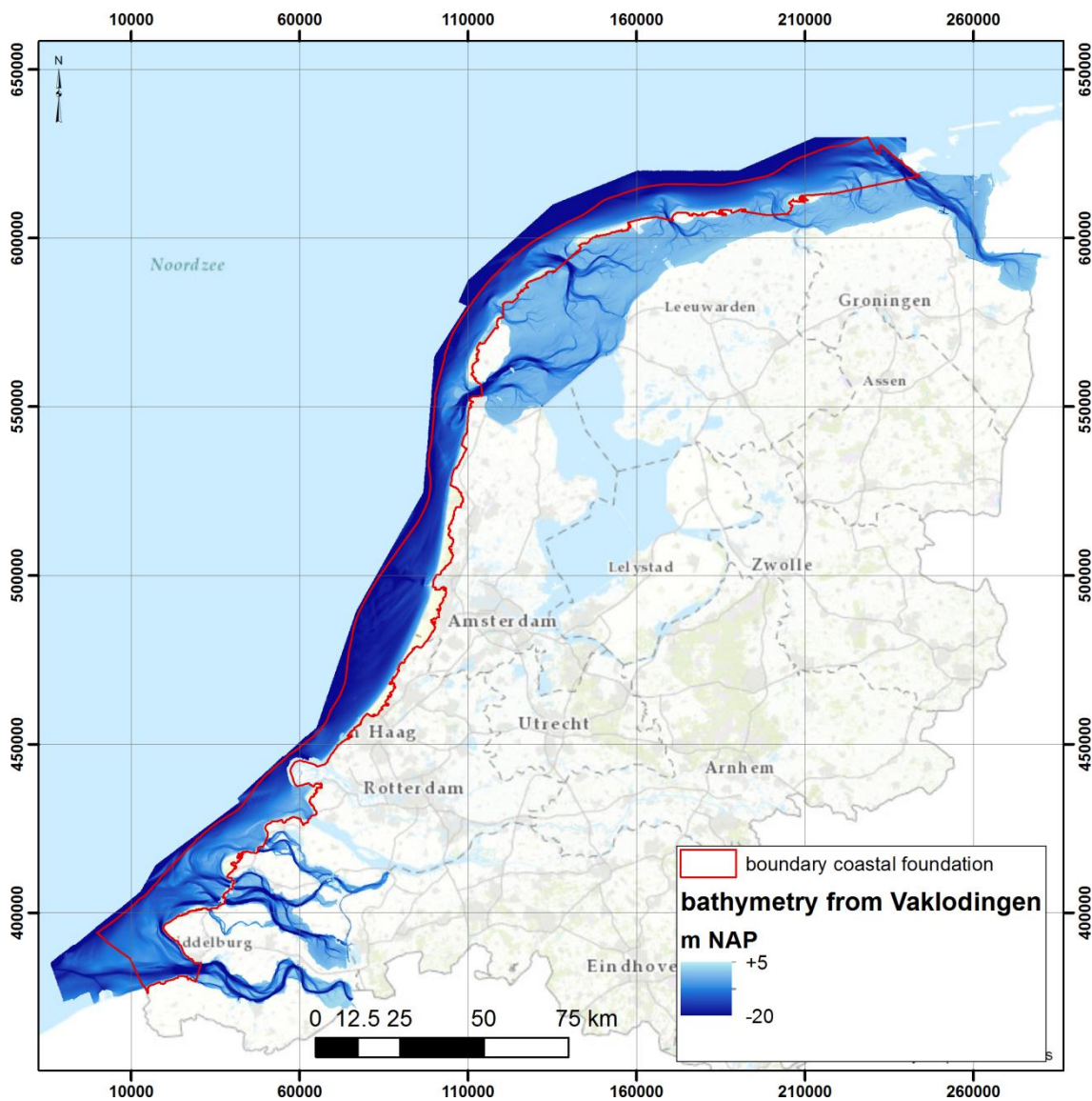


Figure 2.2. Coastal foundation boundaries overlaying the bathymetry from Vaklodgingen measurements between 2009 and 2014.

The coastal foundation is maintained by means of sand nourishments. Currently, the total yearly nourishment volume Q_{nour} follows from (Lodder, 2016):

$$Q_{nour} = A_{KF} * SLR + losses = (A_{KF} + A_{WS} + A_{WZ}) * SLR \quad (2.1)$$

where A_{KF} , A_{WS} , A_{WZ} are the areas of the coastal foundation, Western Scheldt and Wadden Sea basins, respectively, and SLR the actual sea level rise. This equation assumes negligible onshore, offshore and lateral losses, does not account for land subsidence and computes the import into the Western Scheldt and Wadden Sea by multiplying the basin area with the sea level rise. For example, with $A_{KF} = 4181 \text{ km}^2$, $A_{WS} = 253 \text{ km}^2$ (Dutch part only), $A_{WZ} = 2497 \text{ km}^2$ and $SLR = 0.18 \text{ cm/year}$ (Baart et. al., 2015) the nourishment volume is 12.5 million m^3/year , which is actually nourished every year since 2000 (Lodder, 2016).

Recent studies showed that some assumptions behind Eq. (2.1) might not be valid. Especially, the sediment loss to the Wadden Sea is likely to be higher than the area of the Wadden Sea basin multiplied with sea level rise, because of morphological adaptations to the closure of the Zuiderzee (1932) and Lauwerszee (1969) and subsidence due to gas and salt mining. Therefore, in the same paper Lodder (2016) proposed the following extended expression to compute the yearly nourishment volume:

$$Q_{nour} = A_{KF,new} * SLR + Q_{loss,basins} + Q_{loss,mining} + Q_{loss,borders} \quad (2.2)$$

With A_{KF} the coastal foundation area with new offshore boundaries and terms accounting for the net sediment loss into the Western Scheldt and Wadden Sea basins, sediment loss within the KF due to subsidence related to gas and other extractions, and net sediment loss to Belgium and Germany. This expression still assumes no net sediment transport across the offshore and onshore boundaries of the coastal foundation. Modifying the on- and offshore boundaries and hence the surface area of the coastal foundation can result in a different A_{KF} -used in (Eq. 2.1). ENW (2017) gave a positive advice about this Lodder (2016) formulation to determine the nourishment volume, and to serve as a basis for the KG-2 research programme.

The hydrodynamic conditions on the shoreface result from tide-, wind- and density gradient driven currents and the wave-induced orbital motion. Van der Werf et al (2017) describe these processes in more detail.

3 Methods to calculate transport at shoreface

To provide input to the above consideration, the sediments transports across the offshore boundaries need to be assessed. To assess the relative importance of different conditions and transport mechanisms the method to calculate these transports should include effects of tide-, wind-, density gradient driven currents and the skewed wave-induced orbital motion. We propose a method in which the tide-, wind-, density gradient driven currents are calculated with a 3D model, the waves are obtained from observations using a wave transformation matrix and transports are computed with a 1DV transport model.

This is an offline approach, which is relatively fast and easily facilitates assessing the relative importance of the different transport mechanisms, e.g. by artificially modifying density effects (for example by turning it off in the 3D model) or wave skewness effects (for example by manually changing it in the 1DV transport model) and makes sensitivity calculations by changing parameter settings relatively easy. It also facilitates application of different transport formulations.

Impact of the waves on the stratification and flow is not taken into account in this offline approach. Comparison with an online approach will therefore also be made in a later stage.

Tide-, wind-, density gradient driven currents are obtained from the 3D Dutch Continental Shelf Model-Flexible Mesh model (3D DCSM-FM). We will briefly describe the main characteristics of the 3D DCSM-FM model here. Details are presented by Zijl and Veenstra (2018). Wave conditions are obtained from a wave transformation matrix (De Fockert and Luijendijk, 2011). The wave transformation matrix will also be described briefly.

To assess the annual transports, sediment transport computations are performed using the 1DV model by Van Rijn et al. (2018). It is an engineering approach of the Van Rijn (2007) model and described in more detail in appendix A. The sediment transport model requires flow and wave conditions as an input.

To test our numerical approach, two locations along the Noordwijk transect have been selected, i.e. NOORDWK10 and NOORDWK20. These are default output locations stations in the 3D DCSM-FM model and in one of the transects for which the model was validated (see Zijl and Veenstra, 2018). Van Rijn (1997) also presents transports in the Noordwijk transect, in addition to three other locations along the central Dutch coast, which makes it possible to compare our results with those by Van Rijn (1997).

3.1 3D Dutch Continental Shelf Model-Flexible Mesh (3D DCSM-FM)

Stratification caused by the freshwater outflow of the Rhine alters the tidal currents in front of the Dutch coast. The top and bottom layers of the flow become decoupled due to stratification. A cross-shore sediment transport may be caused by stratification. Research has shown that this is indeed the case (see e.g. Hop, 2017). Therefore, to answer the two main questions of the KG2 project it is important to model the effect of stratification on the velocity field. This can be done with the 3D DCSM-FM model. The model includes the tide, wind and discharge. The 3D DCSM-FM model has originally been setup as part of Deltares' strategic research funding, with a focus on long-term water quality. Since then this model has been used for numerous studies.

Figure 3.1 shows the 3D DCSM-FM model grid. The DCSM-FM network was designed to have a resolution that increases with decreasing water depth. Figure 3.2 shows DCSM-FM model bathymetry in the southern North Sea. Zijl and Veenstra (2018) provide details on the set-up and validation of the 3D DCSM-FM model.

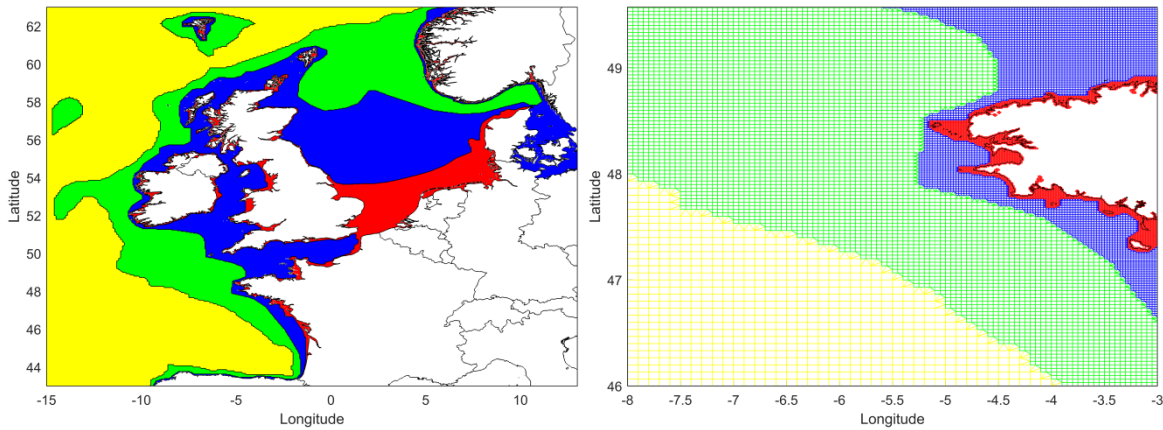


Figure 3.1. Overview (left) and detail (right) of the 3D DCSM-FM model network with the colours indicating the grid size (yellow: ~4 nm; green: ~2 nm; blue: ~1nm; red: ~0.5 nm).

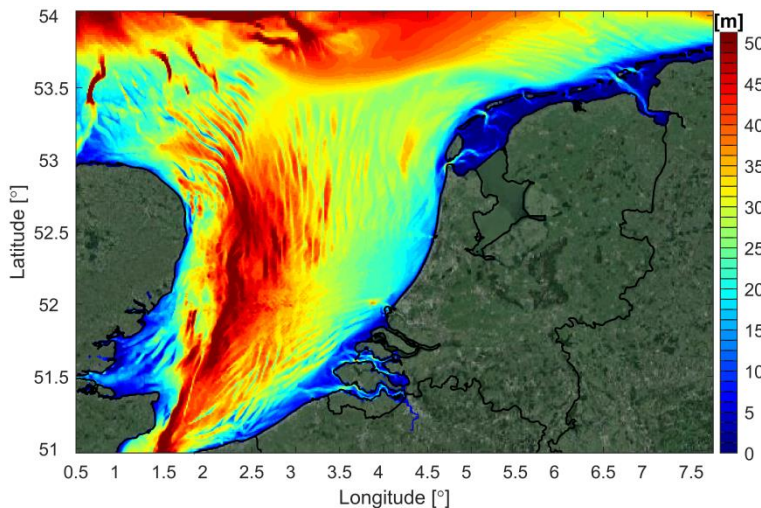


Figure 3.2. DCSM-FM model bathymetry in the southern North Sea (depths relative to MSL).

3.2 Wave transformation matrix

Wave conditions are obtained from a wave transformation matrix, or wave look-up table, that transforms measured offshore wave time series from the IJmuiden, Europlatform, Eierlandse Gat and Schiermonnikoog North waverider stations to an arbitrary location nearshore (see **Error! Reference source not found.**).

The wave transformation matrix uses the following parameters:

- a) wave height (H_{m0}),
- b) mean period (T_{m02}),
- c) wave direction (nautical coordinates),
- d) wind speed,
- e) wind direction
- f) surge

Figure 3.3 shows an example of the validation with observations at Meetpost Noordwijk. Wave heights and wave periods show good agreement with the observations.

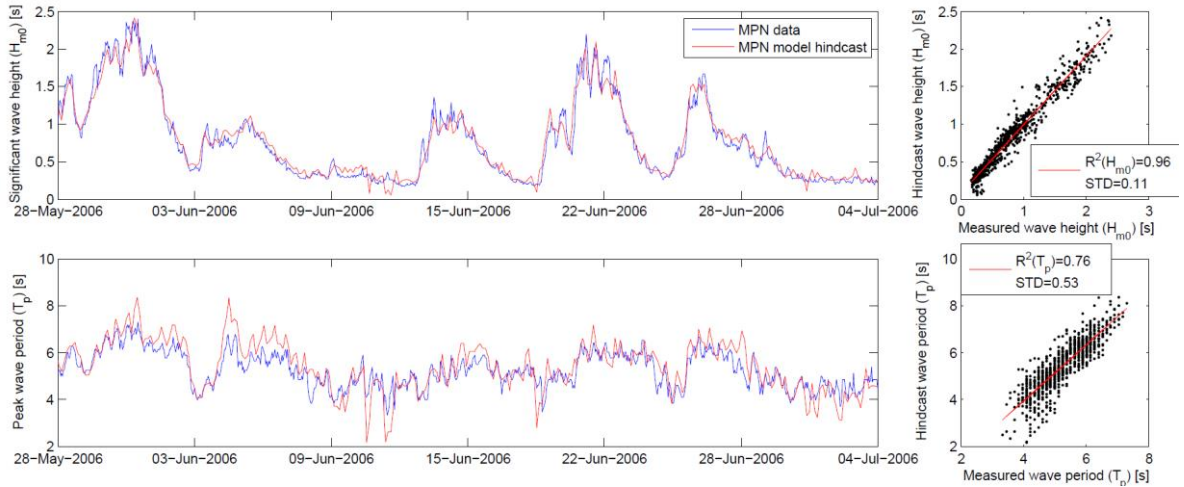


Figure 3.3 Observed wave height and wave period and hindcast from wave transformation matrix for Meetpost Noordwijk (MPN)

More details on the wave transformation matrix are provided by De Fockert and Luijendijk (2011).

3.3 Sediment transport model

The sediment transport rates are computed with the TSAND model. Appendix A describes the transport model in detail. Here we summarize the main characteristics.

TSAND is a simplified sand transport model for tidal flow with waves. The simplified approach is based on the detailed sediment transport formulations by Van Rijn (1984, 1993, 2007, 2015), which have been verified extensively.

The TSAND-model can be used standalone or as a post-processing model to compute the instantaneous variation of the depth-integrated suspended sand transport and total transport (incl. bed-load transport). Here we use it as a post-processing model to compute annual transports.

3.3.1 Suspended sand transport

The suspended sand transport is computed by integration of the product of velocity and concentration over the water depth:

$$q_s = \int_a^h (uc_{sand}) dz$$

The velocities (u) and sand concentrations (c_{sand}) are computed as a function of height above bed and time. The grid points over the depth (50 points) are distributed exponentially. Used standalone, the basic hydrodynamic parameters should be specified by the user. Used as a post-processing model, the hydrodynamic input may come from a 1D, 2DH or 3D-model.

The sand concentration profile is represented as:

$$c_{sand} = c_{a,sand} \left[\left(\frac{h-z}{z} \right) \left(\frac{a}{h-a} \right) \right]^{ZS}$$

with: c_{sand} = sand concentration (kg/m^3), $c_{a,sand}$ = reference sand concentration (kg/m^3), h = depth (m), z = height above bed (m), a = reference height above bed (m), ZS = dimensionless suspension number of sand.

The suspension number ZS of sand is represented as:

$$ZS = \frac{w_{sand,0}}{\beta \kappa u_{*,cw}} + 2.5 \left(\frac{w_{sand,0}}{u_{*,cw}} \right)^{0.8} \left(\frac{c_{a,sand}}{c_0} \right)^{0.4} + \left(\frac{\rho_{sa}}{\rho_{fresh}} - 1 \right)^{0.4}$$

with: $w_{sand,0}$ = fall velocity of single sand particle based on d_{50} , κ 0.4, $\beta = 1 + 2(w_{sand,0} / u_{*,cw})^2$ = coefficient with maximum of 1.5, $u_{*,cw} = (u_{*,c}^2 + u_{*,w}^2)^{0.5}$ = bed-shear velocity due to current and waves, $u_{*,c} = (\tau_{b,c} / \rho)^{0.5}$ = current-related bed-shear velocity, $u_{*,w} = (\tau_{b,w} / \rho)^{0.5}$ = wave-related bed-shear velocity, $c_{a,sand}$ = total reference concentration, $c_0 = 0.65$ maximum bed concentration, ρ fluid density including salinity effects, ρ_{fresh} fluid density of fresh water (= 1000 kg/m³).

The suspension number represents the effects of downward gravity settling, upward turbulence mixing (first term), damping due to vertical sediment concentration gradients (second term) and damping due to vertical salinity gradients (third term), (Winterwerp 2001; Van Rijn 1984, 1993, 2007).

3.3.2 Bedload sand transport

The bed load transport can be computed with two different methods.

3.3.2.1 Bedload transport method 1

The first method includes the effect of wave skewness and computes the bedload transport based on the quasi-steady approach by Van Rijn (2007) as follows:

$$q_b = \int_0^T q_{b,t} dt$$

with $q_{b,t}$ the intra-wave time-dependent bedload transport and T the wave period.

The intra-wave time-dependent bedload transport is computed as follows:

$$q_{b,t} = \gamma \rho_s f_{silt} d_{50} D_*^{-0.3} \left(\frac{\tau_{b,cw,t}}{\rho} \right)^{0.5} \left(\frac{\tau_{b,cw,t} - \tau_{cr}}{\tau_{cr}} \right)^\eta$$

with $\tau_{b,cw,t} = 0.5 \rho_w f_{cw} U_{\delta,cw}^2$ = intra-wave time-dependent grain-related shear stress due to both waves and currents, $f_{cw} = \alpha \beta f_c + (1 - \alpha) f_w$ = grain friction coefficient due to currents and waves, $f_c = 8g / (18 \log(12h / k_{s,grain}))^2$ = current-related grain friction coefficient, $k_{s,grain} = d_{90}$, $f_w = \exp(-6 + 5.2(A_w / k_{s,grain})^{-0.19})$ = wave-related grain friction coefficient, $\alpha = u_c / (u_c + U_w)$ = coefficient relative strength of wave and current motion, u_c = depth-averaged current velocity, U_w = peak orbital velocity, β = coefficient related to vertical structure of velocity profile (Van Rijn, 1993); h = water depth. $\tau_{b,cr}$ = critical bed shear stress, ρ_s = sediment density, d_{50} = median particle diameter, $D_* = d_{50}((s-1)g / \nu^2)^{1/3}$ = dimensionless particle size, s = relative density, ν = kinematic viscosity, $f_{silt} = d_{sand} / d_{50}$ = silt factor ($f_{silt} = 1$ for $d_{50} > d_{sand}$), γ = calibration coefficient = 0.5, η = calibration coefficient = 1.

For the quasi-steady bedload transport approach, the intra-wave near-bed velocity is computed based on the parameterization by Isebe and Horikawa (1982).

3.3.2.2 *Bedload transport method 2*

The second bedload transport method does not include the effect of wave skewness and is based on the simplified expression by Van Rijn (2007) as follows:

$$q_b = 0.015 \rho_s u h \left(\frac{d_{50}}{h} \right)^{1.2} (M_e)^{1.5}$$

with: q_b = depth-integrated bed-load transport (kg/s/m); $M_e = (u_e - u_{cr}) / [(s-1)gd_{50}]^{0.5}$; $u = u + \gamma U_w$ = effective velocity with $\gamma = 0.4$ for irregular waves and $\gamma = 0.8$ for regular waves, u = depth-averaged flow velocity; $U_w = \pi H_s / (T_p \sinh(kh))$ peak orbital velocity; H_s = significant wave height (m); T_p = wave spectrum peak period (s); u_{cr} = critical depth-averaged velocity (m/s), d_{50} = median grain diameter (m), h is the water depth (m).

3.3.3 Total load transport

The total load transport of sand is computed as the sum of the suspended load and bed load.

4 Validation of method at Noordwijk

Firmijn and Veenstra (2018) validated the 3D DCSM-FM model for the calendar years 2013-2016. The model output of these series of model runs was used here to set-up our offline approach to calculate the sediment transport rates at the lower shoreface and make first preliminary calculations for two locations. Flow output has been generated every 10 minutes at NOORDWK20 and NOORDWK10. Here we will show characteristics examples of profiles and moving averages of time series or statistical representations of these time series. We will then describe the wave characteristics for this years based on the wave transformation matrix output. Finally, we will describe the resulting transport rates at these two locations and make a comparison with earlier studies.

4.1 Flow and salinity

Figure 4.1 shows the tide-averaged values of the computed velocities near the bed (bottom layer) and near the water surface (top layer) at NOORDWK20 for the years 2013, 2014, 2015 and 2016. This figure shows the spring-neap tidal variations of the velocities with larger velocities during spring tide and smaller velocities during neap tide. The velocities near the bed are always smaller than near the surface due to bottom friction. It is interesting to see also that the variations of the velocities near the surface are larger than near the bed, which is due to variations in wind force and wind direction. Velocities near the bed are less affected by wind.

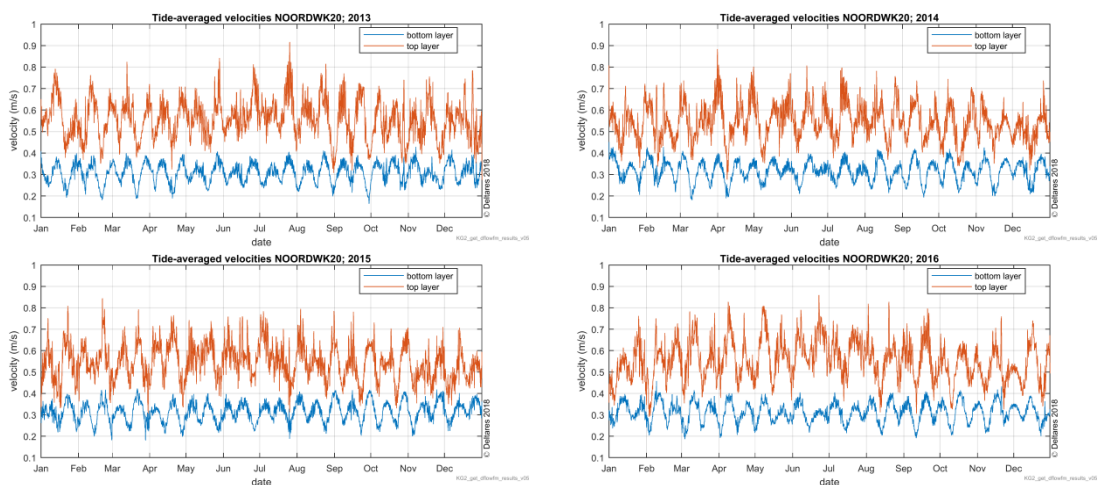


Figure 4.1 Tide-averaged velocities near bed and water surface at location NOORDWK20 for 2013, 2014, 2015 and 2016

Figure 4.2 shows the computed salinities near the bed (bottom layer) and near the surface (top layer) at NOORDWK20 for the years 2013, 2014, 2015 and 2016. Salinity variations are mainly due to Rhine fresh water discharge variations. Figure 4.2 shows that salinities may vary daily, monthly and seasonally but also vary from year to year. On average, in 2013 the salinity was smaller (less saline) at NOORDWK20 than in the other years for example. The average difference in salinity between the top layer and the bottom layer (measure of stratification) was also stronger in this year.

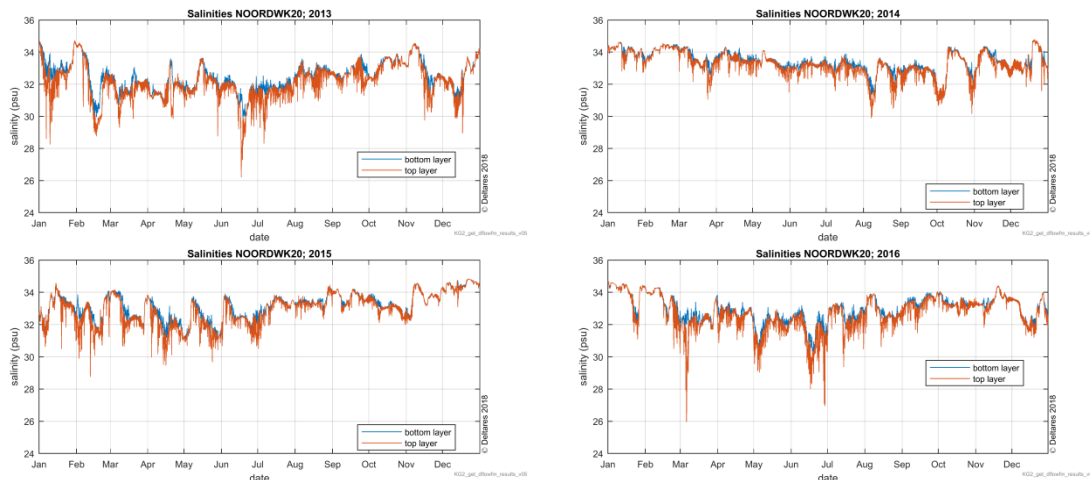


Figure 4.2 Salinities near bed and water surface at location NOORDWK20 for 2013, 2014, 2015 and 2016

To illustrate the effect of salinity stratification on the velocity profile, Figure 4.3 shows the computed velocity and salinity profiles for rising tide under relatively calm conditions at NOORDWK20. The velocity profile in the top left panel is not logarithmically distributed as would have been expected without stratification effects. In contrast, the near-bed velocities in x direction (latitudinal) are larger and in y direction (longitudinal) smaller. This is caused by the stratified salinity profile shown in the top right panel. More saline water near the bed tends to flow towards the coast. This stratified flow generally occurs under relatively calm conditions.

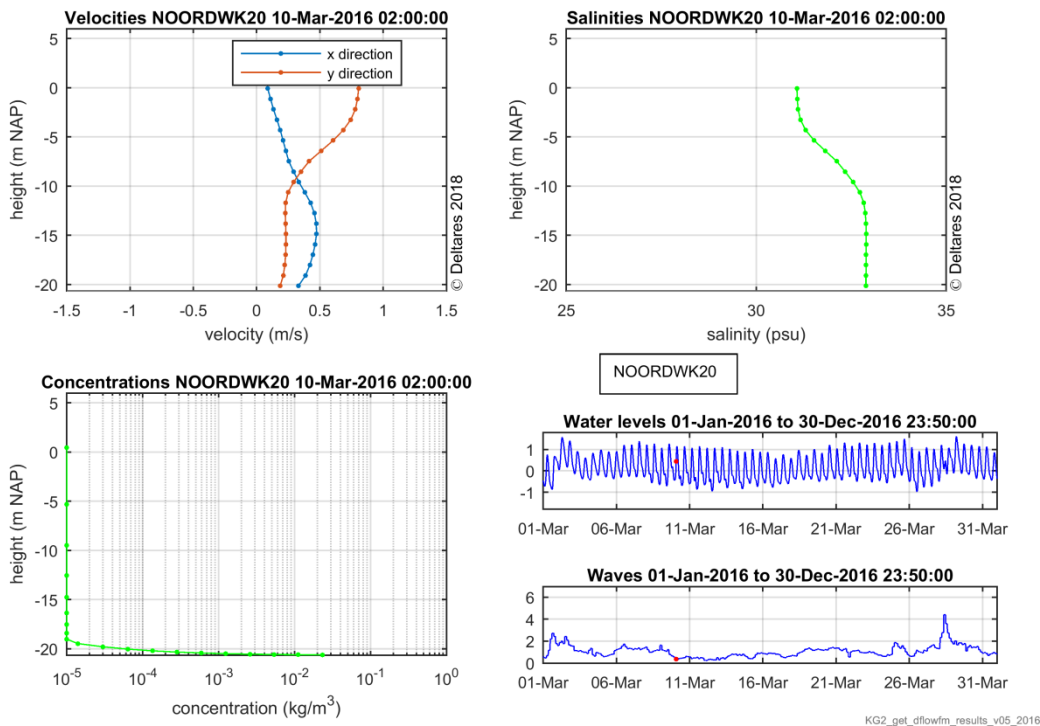


Figure 4.3 Computed parameters at NOORDWK10 for rising tide under calm conditions on 10 March 2016. Top left: velocity profile in x direction (latitudinal) and y direction (longitudinal), top right: salinity profile, lower left: concentration profile, lower right: water levels and waves.

Figure 4.4 shows the computed velocity and salinity profiles for rising tide under more energetic conditions at NOORDWK20. The velocity profiles (top left) show a logarithmic distribution without stratification effects. The computed salinity profile (top right) shows a uniform distribution over depth.

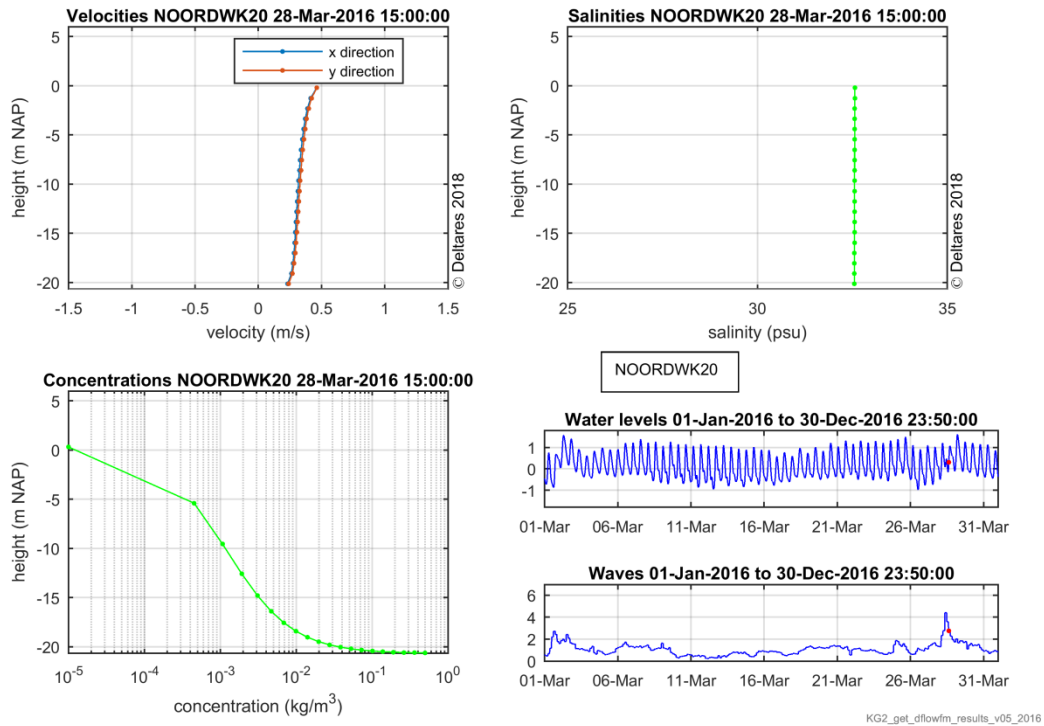


Figure 4.4 Computed parameters at NOORDWK10 for rising tide under energetic conditions on 28 March 2016. Top left: velocity profile in x direction (latitudinal) and y direction (longitudinal), top right: salinity profile, lower left: concentration profile, lower right: water levels and waves.

4.2 Waves

Wave conditions may vary from year to year. In some years more storms can occur than in others. Although the average wind direction in the Netherlands is approximately southwest, wind directions during storms can vary per storm and per year.

Figure 4.5 shows the wave roses for years 2013-2016 at Noordwijk, derived with the wave transformation matrix. Dominant wave directions are southwest and northwest for all four years. The year 2013 was the calmest of the four. The years 2015 and 2016 were stormier than 2013 and 2014. More NW storms and less SW storms occurred in 2016 than in 2015. See wave time series in appendix C and joint occurrence tables in appendix D.

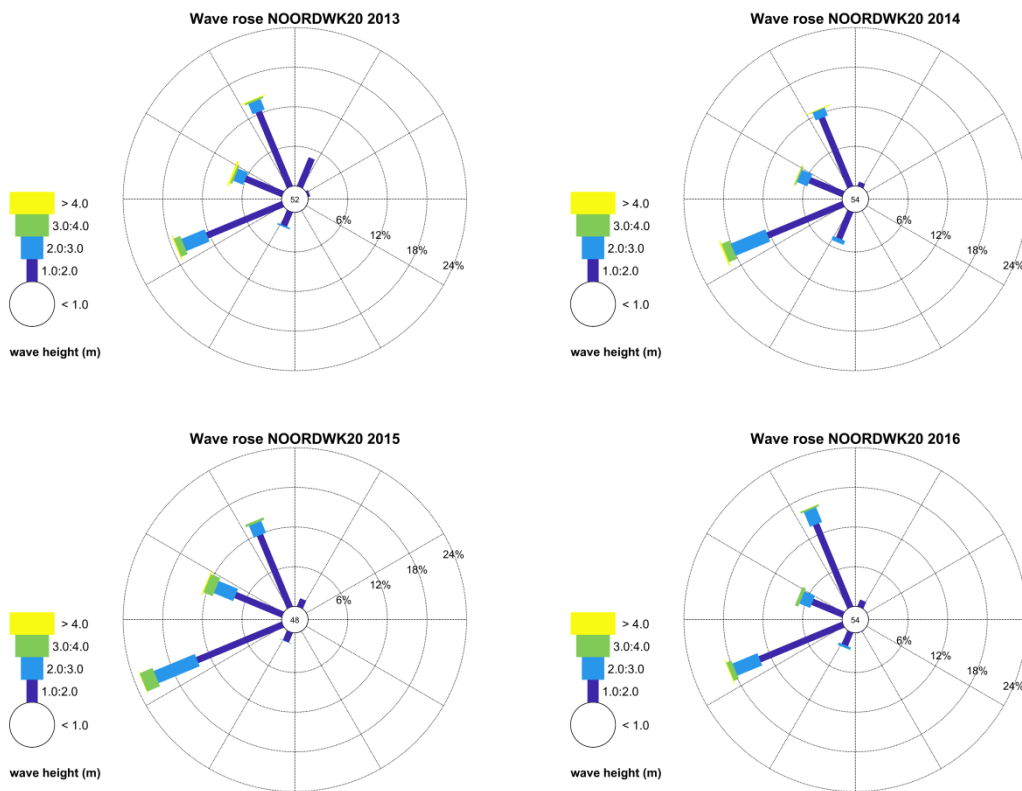


Figure 4.5 Wave roses at location NOORDWK20 for 2013, 2014, 2015 and 2016 from wave transformation matrix.

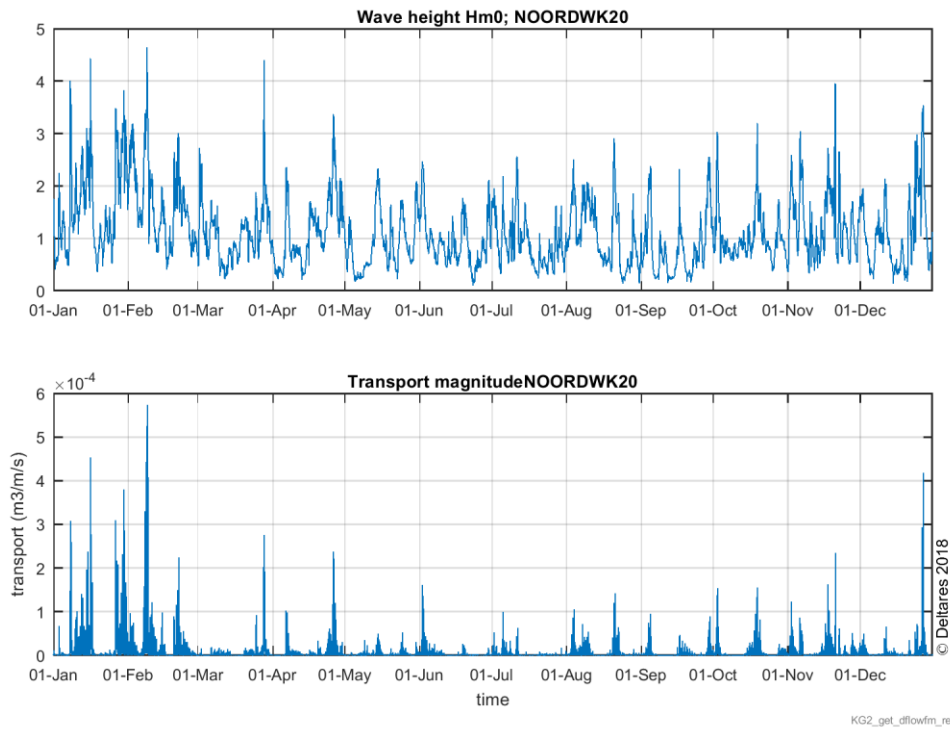
4.3 Annual transports rates

To test our numerical approach, we have made sediment transport computations at locations 20 km and 10 km off the coast of Noordwijk aan Zee (NOORDWK20 and NOORDWK10) for the years 2013-2016 with the 1DV Van Rijn et al. (2018) transport model using flow conditions from the 3D DCSSM-FM model and wave conditions from the wave transformation matrix. Main parameters settings are presented in the table below. All calibration factors were set to default values (no calibration done). Water depths at NOORDWK20 and NOORDWK10 are about 21 m and 19 m, respectively.

Parameter	Value
Reference height a	0.05 m
D_{10}	100 μm
D_{50}	250 μm
D_{90}	400 μm
Sand fraction p_{sand}	0.97
Mud fraction p_{mud}	0.03
Dry bed density ρ_{dry}	1590 kg/m^3
Coast angle Noordwijk	27.92°

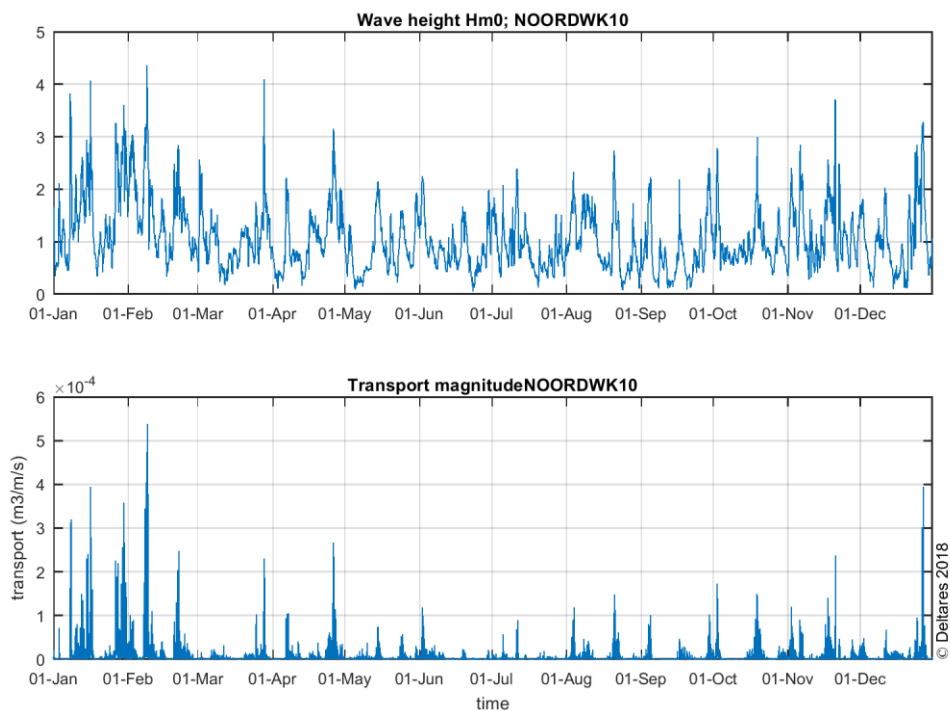
As an example, Figure 4.6 shows the wave heights from wave transformation matrix (top panel) and the computed instantaneous transport rates (lower panel) for the year 2016 at NOORDWK20. Figure 4.7 shows the same for NOORDWK10. At these locations, transport rates are negligibly small for H_{m0} smaller than about 1 m, which occurs about 50% of the year. Transport rates become significant for H_{m0} of 1-2 m, which occurs about 40% of the year and are largest for $H_{m0} > 2$ m, which occurs about 10% of the year (see appendix D for

wave statistics). Relative contributions of different conditions and transporting mechanisms to the total sediment transport at different water depths will be made in a later project phase.



KG2_get_dfflowfm_results_v05_2016

Figure 4.6. Wave height from wave transformation matrix (top panel) and computed instantaneous transport rate (lower panel) for the year 2016 at NOORDWK20



KG2_get_dfflowfm_results_v05_2016

Figure 4.7. Wave height from wave transformation matrix (top panel) and computed instantaneous transport rate (lower panel) for the year 2016 at NOORDWK10

Figure 4.8 shows the computed annual net sand transport at NOORDWK20 and NOORDWK10 for each year separately based on a median grain diameter D_{50} of 250 μm . The transports at NOORDWK20 are mainly alongshore directed due to the tidal flow directions. Transports at NOORDWK10 are also mainly alongshore directed but tend to have an onshore component as well.

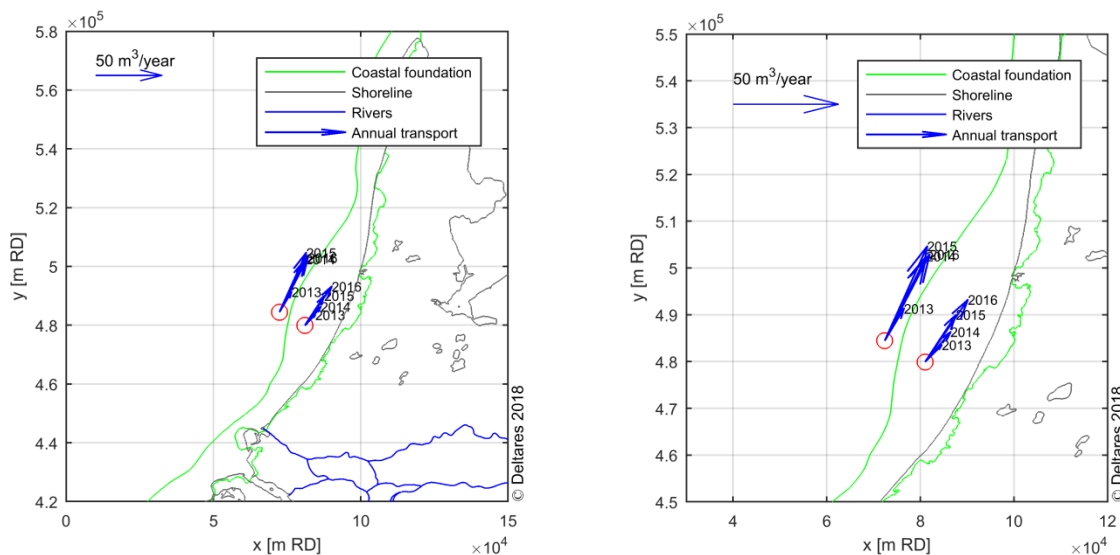


Figure 4.8. Computed annual transport vectors for the years 2013 to 2016 (left) and zoom in (right). Top left arrow shows the vector scale.

Assuming a coast angle of 27.92° at Noordwijk we decomposed the annual transport vectors into an alongshore and a cross-shore component. We should note here that assuming this coast angle for locations just offshore of the coastal foundation contour at Noordwijk may lead to an underestimation of the “onshore” transports as the 20 m depth contour has a smaller angle relative to the north here.

4.3.1 Alongshore transport rates

Figure 4.9 shows the computed annual alongshore transport for 2013, 2014, 2015 and 2016 at NOORDWK20 (upper panel) and NOORDWK10 (lower panel) for a D_{50} of 250 μm and 280 μm .

Using a D_{50} of 250 μm , the computed total alongshore transport rate at NOORDWK20 averaged over all four years amounts to 35 m^3/year and varies between 16 m^3/year in 2013 and 44 m^3/year in 2015. The computed total alongshore transport at NOORDWK10 averaged over all four years amounts to 21 m^3/year and varies between 10 m^3/year in 2013 and 32 m^3/year in 2016.

4.3.2 Cross-shore transport rates

Figure 4.10 shows the computed annual cross-shore transports for 2013, 2014, 2015 and 2016 at NOORDWK20 (upper panel) and NOORDWK10 (lower panel).

Using a D_{50} of 250 μm , the computed annual cross-shore transport at NOORDWK20 Averaged over all four years amounts to -1 m^3/year (offshore directed) and varies between -3 m^3/year (offshore) in 2015 and +1 m^3/year (onshore) in 2013.

Averaged over all four years the computed annual cross-shore transport at NOORDWK10 is +3 m^3/year (onshore) and here it varies between 2 m^3/year in 2015 and 4 m^3/year in 2016.

The variations in computed annual transports are relatively large (Figure 4.9). At both locations the standard deviation is about 40-50% of the mean over the years. This variation per year is larger than the effect of using a D_{50} of 280 μm instead of a D_{50} of 250 μm in the computations.

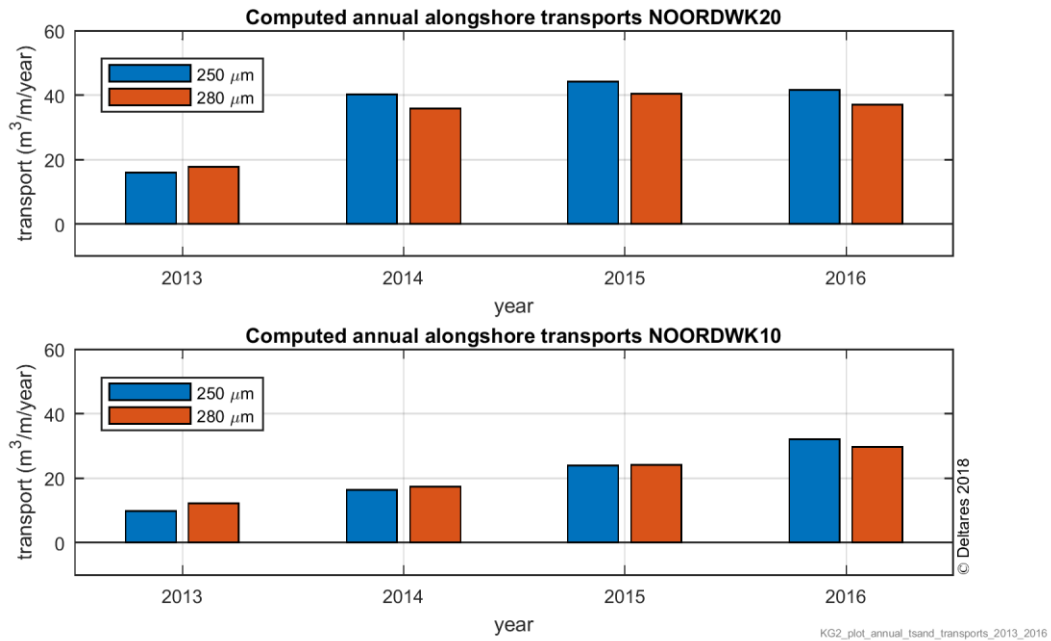


Figure 4.9. Computed annual alongshore transports for the years 2013 - 2016 at NOORDWK20 (upper) and NOORDWK10 (lower) for $D_{50} = 250 \mu\text{m}$ and 280. Water depths at NOORDWK20 and NOORDWK10 are about 21 m and 19 m, respectively.

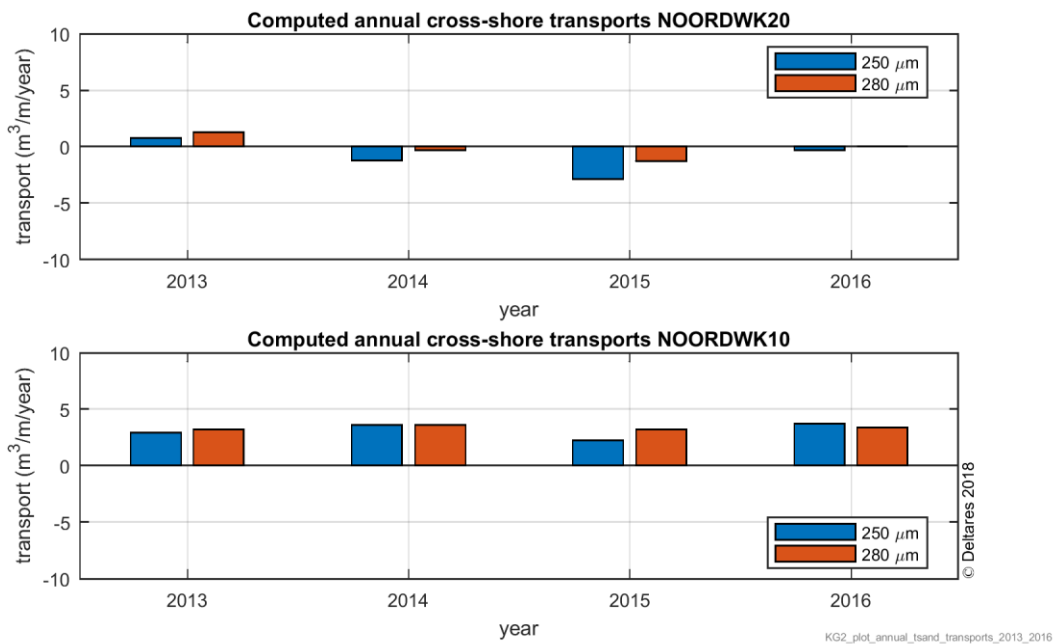


Figure 4.10. Computed annual cross-shore transports for the years 2013 - 2016 at NOORDWK20 (upper) and NOORDWK10 (lower) for $D_{50} = 250 \mu\text{m}$ and 280. Water depths at NOORDWK20 and NOORDWK10 are about 21 m and 19 m, respectively.

The table below compares the alongshore and cross-shore transport rates computed by Van Rijn (1997) and computed here. We combined the results of NOORDWK20 and NOORDWK10 for the four years to have an estimate of the transport around the NAP-20 m depth contour.

Van Rijn (1997) computed the sediment transport of the central coastal zone of Holland at the NAP -8 m and the NAP -20 m contour using a 1D approach in a direction normal to the shore at 4 different transects. The annual sediment transport rates were computed with schematized wave and corresponding current conditions. The tide was represented by one representative tide and the waves by 3 different wave height classes from 8 different directions.

In contrast to the Van Rijn (1997) approach, no schematization of the flow and wave climate has been made in our 3D offline approach. The actual currents and waves have been applied, which is physically more realistic and complete. In addition, the large 3D model facilitates application on wider temporal and spatial dimensions. More and other periods can be selected and arbitrary locations along the entire Dutch coast can be chosen.

The average alongshore transport rates computed here are within the bandwidth of transports estimated by Van Rijn (1997). The cross-shore transports are much smaller than those estimated by Van Rijn (1997). Hop (2017) also found cross-shore transport rates much smaller than those estimated by Van Rijn (1997) and argues that the difference may be due to way the density effect is taken into account and due to the sediment transport formulations applied.

Table 4.1 Computed mean annual transport rates ($m^3/m/year$)

	Van Rijn (1997)	Computed here (average NOORDWK10 and NOORDWK20; 2013-2016)
Alongshore at 20 depth	35 ± 15	28 ± 16
Cross-shore at 20 depth	10 ± 10	1 ± 4

5 Discussion, conclusions and recommendations

5.1 Discussion

Similar to this study, Hop (2017) also found cross-shore transport rates much smaller than those estimated by Van Rijn (1997) and argues that the difference may be due to way the density effect is taken into account and due to the sediment transport formulations applied.

Van Rijn used a single value to schematize the density current for the entire Holland coast (Vermaas, 2010). Other studies indicate however that the effect of the density current is decreasing in northward direction (De Ruijter et al., 1997; De Boer, 2009; Hop, 2017). The impact is largest near the river mouth and decreases in northward direction. Hop (2017) found the stratification effects in the range of $-2 \text{ m}^3/\text{m}$ to $2 \text{ m}^3/\text{m}$, which is comparable to the effect found here but an order of magnitude smaller than the results of Van Rijn (1997).

With respect to the density effect, the small difference found here between the cross-shore transport rates at NOORDWK20 and NOORDWK10 is interesting. Figure 5.1 shows the wave heights in the year 2016 and the computed ratio between the salinity in the bottom layer and that in the top layer. The latter may be seen as a measure for density stratification: 1 means no stratification and > 1 means stratified. Figure 5.1 shows a small difference in stratification between NOORDWK20 and NOORDWK10, particularly in the periods during which stratification is present. It appears that stratification occurs slightly more often at NOORDWK10 than at NOORDWK20 and also that the stratification at NOORDWK10 occurs more during periods of higher waves, in Figure 5.1 for example at the beginning of February and July.

This seems to indicate that stratification has a subtle effect on the transport rates but is important to take into account in computing the annual sediment transport rate.

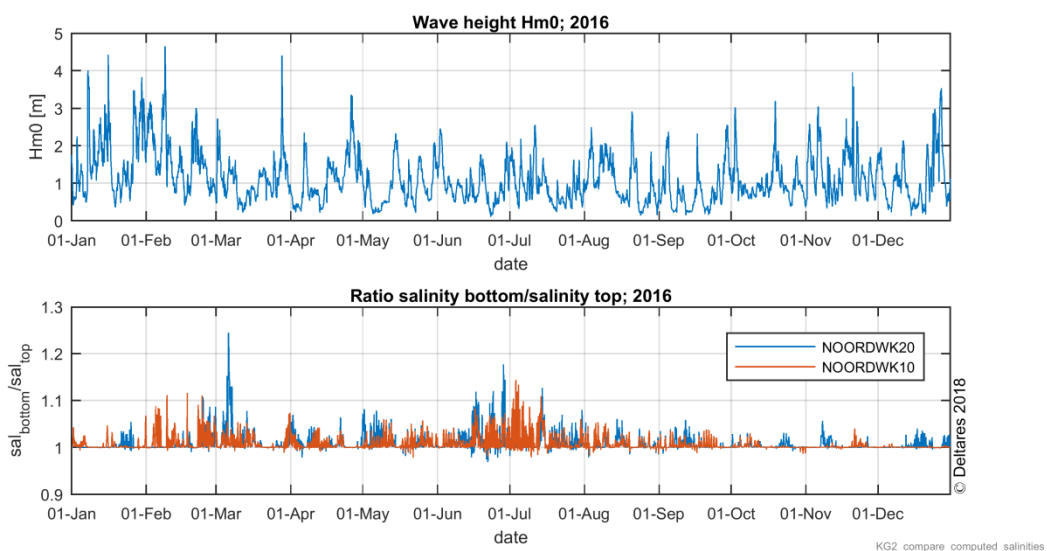


Figure 5.1. Wave height in the year 2016 (top panel) and computed salinity ratio between bottom layer and top layer (lower panel)

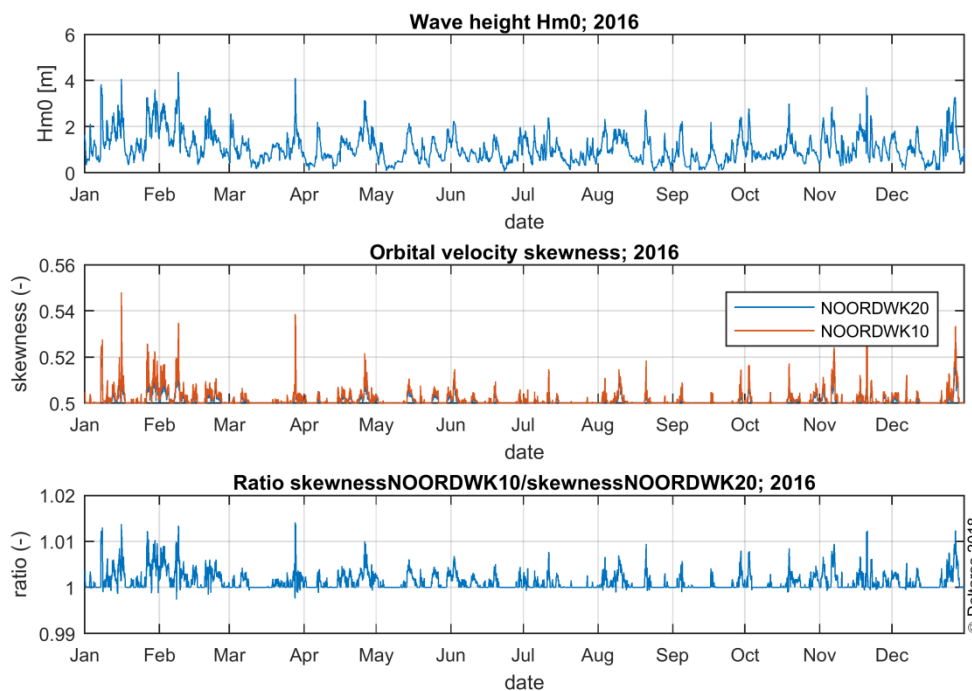
An aspect that may also affect the cross-shore transport rate is the orbital velocity skewness, defined as follows:

$$R_u = \frac{u_{\max}}{u_{\max} + u_{\min}}$$

Because the maximum positive ('onshore') velocity u_{\max} , exceeds the maximum negative ('offshore') velocity u_{\min} , R_u generally exceeds 0.5 (Ruessink et al, 2012). Under natural conditions, R_u typically varies between 0.5 and 0.7 (Elfrink et al., 2006).

As an example of the skewness values at the lower shoreface, Figure 5.2 shows the wave height in the year 2016 at NOORDWK10, computed orbital velocity skewness at NOORDWK20 and NOORDWK10 and the ratio between the two. This figure shows that the orbital velocities are generally slightly skewed both at NOORDWK20 and NOORDWK10 and that the skewness at NOORDWK10 is slightly larger than at NOORDWK20.

This indicates that also the orbital velocity skewness has a subtle effect on the transport rates and is important to take into account in computing the annual sediment transport rate.



KG2_get_dflowfm_results_v05_2016

Figure 5.2. Wave height in the year 2016 (top panel), computed orbital velocity skewness for NOORDWK20 and NOORDWK10 (middle panel) and ratio skewnessNOORDWK10/skewnessNOORDWK20 (lower panel)

The applied sediment transport model and the way in which the input is schematized may also have an impact on the results (Hop, 2017; Waagmeester, 2015). For example, Van Rijn (1997) applied a 2 DV cross-shore model (Unibest) with the Van Rijn (1993) suspended transport model in combination with the Ribberink (1997) bedload transport model and schematized the tide by one representative tide and discrete wind and wave classes. Waagmeester (2015) found the same results as Van Rijn (1997) with the energetic approach sediment transport formulations and found the same results as Hop (2017) and also the same as in this study when using the Soulsby-Van Rijn formula. The effect of different sediment transport formulations has not been studied here.

5.2 Conclusions

We have developed and tested an offline Sediment Transport Model for the Dutch Lower Shoreface that can compute annual sand transport rates at arbitrary locations along the lower shoreface of the Dutch coast. The approach is based on output of the state-of-the-art 3D DCSM-FM model, wave observations together with a wave transformation matrix for the Dutch coast and a 1DV sand transport module.

The average annual alongshore transport rates computed here at the Noordwijk transect encouragingly agree with the bandwidth presented by Van Rijn (1997) for the same transect.

The average annual cross-shore transport rates computed here agree with estimates by Hop (2017) and Waagmeester (2015) at the Noordwijk transect using the Soulsby-Van Rijn transport formulation but are smaller than the best estimate presented by Van Rijn (1997).

The variation in annual transports is relatively large per year (~40-50%).

The effect of a larger D_{50} is relatively small (~10%) compared to the variation per year.

5.3 Next steps

In the next phase of the project the offline approach will be validated with an online approach. The offline model results will also be compared with flow, wave and transport measurements made at the lower shoreface of Ameland, Terschelling and Noordwijk.

The 3D DCSM-FM model has been extensively calibrated with observed water levels along the entire Dutch coast. The model has been validated with observed mean sea surface salinities and temperatures at the Noordwijk and Terschelling transects. The 3D DCSM-FM model has also been validated with velocities from two measurements buoys located at 27km offshore of Egmond aan Zee and with velocities measured during the Coastal Genesis 2 measurement campaign near Ameland. In the next step, we will validate the velocity profiles also with the velocities measured during the Coastal Genesis campaigns near Terschelling and Noordwijk.

The computations presented here are based on the Van Rijn et al (2018) transport model. To get an indication of the sensitivity due to model uncertainties, in the next step we will make computations also with a different transport model, e.g. Soulsby-Van Rijn (Soulsby, 1997). In addition, we will compare the computed concentrations with those measured during the Coastal Genesis measurement campaign.

The computed annual transport magnitudes and directions on the lower shoreface are fairly sensitive to variations in density stratification. Therefore, in the next step we will investigate the uncertainty bandwidth of computed salinities by comparing the computations with long term observations by Rijkswaterstaat available in the database live.waterbase.nl and with Coastal Genesis 2 measurements at the lower shoreface of Ameland, Terschelling and Noordwijk.

The present model includes wave skewness effects based on the parameterization of Isobe and Horikawa (1982). Ruessink et al. (2012) found the velocity skewness produced by this approach in the nearshore to be considerably larger than that computed with their methodology. Although the area of interest here is focused on the lower shoreface and less on the nearshore, it remains worthwhile in the next step to investigate the effect of the Ruessink (2012) parametrization of the orbital velocities on the computed annual transports. In addition, we will validate the parameterizations with measured orbital velocities.

The net annual transport rates computed in this report are based on hourly flow and wave time series for a limited number of years (four years). Final purpose of the sediment transport computations for the KG2-DV subproject is to assess the long-term annual sediment transport rates across the offshore boundary of the coastal foundation and consequences if an alternative offshore boundary would be chosen. To obtain representative long-term transport rates we will make simulations with this offline approach for 10-20 years in the next step.

We will also investigate the relative contribution of different conditions and transporting mechanisms to the total sediment transport at different water depths (e.g. 12, 14, 16, 18 and 20 m) at different locations along the Dutch coast, including those selected by Van Rijn (1997).

Extreme conditions such as for example a 1/100 storm affect the sediment transport around 15 to 20 m water depth but are not included in the present approach as we use observed conditions. This may be a shortcoming of the present approach. Therefore, in the next step we will include the effect of extreme conditions in the final assessment of transport rates across the offshore boundary of the coastal foundation, for example by simulating synthetic extreme conditions with the 3D DCSM-FM model and computing the transport rates with corresponding extreme wave conditions.

References

- De Fockert, A., Luijendijk, A., 2011. Wave look-up table. Building with Nature. Memo 1002337-002-ZKS-0001. Deltares, Delft, The Netherlands.
- Elfrink, B., Hanes, D.M., Ruessink, B.G., 2006. Parameterization and simulation of near bed orbital velocities under irregular waves in shallow water. *Coastal Engineering* 53, 915–927.
- ENW, 2017. Advies rekenregel suppletievolumen. Brief ENW-17-14 aan het Ministerie van Infrastructuur en Milieu, Directeur-Generaal Ruimte en Water, Expertisenetwerk waterveiligheid.
- Hop, M., 2017. The impact of the Rhine ROFI on the alongshore variability of cross-shore sediment transport of the Holland coast. MSc. Thesis, Delft University of Technology.
- Isobe, M., and Horikawa, K., 1982. Study on water particle velocities of shoaling and breaking waves. *Coastal Engineering in Japan*, 25, 109–123
- Lodder, Q., 2016. Rekenregel suppletievolumen. Rijkswaterstaat Memo.
- Nederbragt, G.J., 2005. Zandvoorraden van het kuststelsel: onderbouwing van een conceptueel model met behulp van trends van de winst- en verliesposten over de periode 1973-1997. Ministerie van Verkeer en Waterstaat, Rijkswaterstaat, Rijksinstituut voor Kust en Zee, RIKZ, 09-2006
- Ribberink, J.S., 1997. Bed-load transport for steady flows and unsteady oscillatory flows. Delft Hydraulics, Delft, The Netherlands.
- Ruessink, B.G., Ramaekers, G., van Rijn, L.C., 2012. On the parameterization of the free-stream non-linear wave orbital motion in nearshore morphodynamic models. *Coastal Engineering* 65, 56–63. <https://doi.org/10.1016/j.coastaleng.2012.03.006>
- Soulsby, R., 1997. *Dynamics of Marine Sands: A Manual for Practical Applications*: Telford.
- Van der Werf, J., Grasmeyer, B, Hendriks, E., Van der Spek A., Vermaas, T., 2017. Literature study Ducth lower shoreface. Report 1220339-004-ZKS-0001. Deltares
- Van Rijn, L.C., 1984a. Sediment Transport, Part I: Bed Load Transport. *Journal of Hydraulic Engineering*, ASCE, Vol. 110, No. 10.
- Van Rijn, L.C., 1984b. Sediment Transport, Part II: Suspended Load Transport. *Journal of Hydraulic Engineering*, ASCE, Vol. 110, No. 11.
- Van Rijn, L.C., 1984c. Sediment Transport, Part III: Bed Forms and Alluvial Roughness. *Journal of Hydraulic Engineering*, ASCE, Vol. 110, No. 12.
- Van Rijn, L.C., 1993. Principles of sediment transport in rivers, estuaries and coastal seas. www.aquapublications.nl
- Van Rijn, L.C., 1997. Sediment transport and budget of the central coastal zone of Holland. *Coastal Engineering* 32, 61–90. [https://doi.org/10.1016/S0378-3839\(97\)00021-5](https://doi.org/10.1016/S0378-3839(97)00021-5)
- Van Rijn, L.C., 1998. Principles of coastal morphology. Aqua Publications, The Netherlands
- Van Rijn, L.C., 2007. Unified view of sediment transport by currents and waves, I, II, III. ASCE, *Journal of Hydraulic Engineering*, Vol. 133, No. 6, 649-667, 668-689, No. 7, 761-775
- Van Rijn, L.C., Grasmeyer, B.T and Perk, L., 2018 Effect of channel deepening on tidal flow and sediment transport; Part I: sandy channels.
- Waagmeester, N. C. D. (2015). Assessing the impact on the annual cross-shore sand transport by the Rhine ROFI at the lower shore face near the Sand Engine. Delft University of Technology, Delft.
- Winterwerp, J.C., 2001. Stratification effects by cohesive and non cohesive sediment. *Journal of Geophysical Research*, Vol. 106, No C10, 22,559-22,574
- Zijl, F., Veenstra, J., 2018. Set-up and validation of 3D DCSM-FM. Memo 1220339-005-ZKS-0003. Deltares, Delft, The Netherlands.

A TSAND model

Introduction

TSAND is a simplified sand transport model for tidal flow with waves. The simplified approach is based on the detailed sediment transport formulations by Van Rijn (1984, 1993, 2007, 2015), which have been verified extensively. The detailed sediment transport formulations have been implemented in the Delft3D-model. The TSAND-model can be used standalone or as a post-processing model to compute the variation of the depth-integrated suspended sand transport and total transport (incl. bed-load transport). It includes the effect of wind waves that may occur in the mouth of a tidal channel. The velocities and sand concentrations are computed as a function of z and t ; z =height above bed and t =time (time step of 5 min). The grid points over the depth (50 points) are distributed exponentially, as follows: $z=a[h/a]^{(k-1)/(N-1)}$ with: a = reference height above bed (input value), $h=h_o+\eta$ = water depth, h_o = depth between bed and mean sea level, η = tidal water level, k = index number of point k , N = total number of grid points. Used standalone, the basic hydrodynamic parameters should be specified by the user. Used as a post-processing model, the hydrodynamic input may come from a 1D, 2DH or 3D-model. TSAND can be used for prismatic and converging channels.

Sand concentrations

The sand concentrations are computed using a single fraction and a multi-fraction method (Van Rijn, 2007). The multi-fraction method is based on $N=6$ sand fractions (0.062-0.125 mm, 0.125-0.2 mm, 0.2-0.3 mm, 0.3-0.5 mm, 0.5-1 mm, 1-2 mm). The sand concentration profile at each time t is represented as:

$$\text{Single fraction: } c_{\text{sand}} = c_{a,\text{sand}} \left[\frac{(h-z)/z}{a/(h-a)} \right]^{ZS} \quad (10a)$$

$$\text{Multi-fraction: } c_{\text{sand},i} = c_{a,\text{sand},i} \left[\frac{(h-z)/z}{a/(h-a)} \right]^{ZS_i} \quad (10b)$$

with: c_{sand} = sand concentration (kg/m^3), $c_{a,\text{sand}}$ = reference sand concentration (kg/m^3), ZS = dimensionless suspension number of sand according to Equation (17), ZS_i = suspension number of sediment fraction i (-).

The reference concentration c_a of the sand fraction is represented as (Van Rijn 1984, 1993, 2007):

$$\text{Single fraction: } c_{a,\text{sand}} = 0.015 \alpha_{ca} (1-p_{\text{mud}}) (d_{50}/a) (T)^{1.5} (D_*)^{-0.3} \quad (11a)$$

$$\text{Multi-fraction: } c_{a,\text{sand},i} = 0.015 \alpha_{ca} (1-p_{\text{mud}}) (d_i/a) (T_i)^{1.5} (D_{*,i})^{-0.3} \quad (11b)$$

with: α_{ca} = correction coefficient (default=1), d_{50} = median particle diameter,
 $D_* = d_{50}[(s-1)g/v^2]^{0.333}$ = dimensionless particle parameter, $D_{*,i}$ = particle parameter of fraction i ,
 $T = (\tau_b/\chi\tau_{b,\text{cr}})/\chi\tau_{b,\text{cr}}$ = dimensionless bed-shear stress parameter,
 $T_i = [\lambda_i(\tau_b/\chi\tau_{b,\text{cr}}\zeta_i)/[\chi(d_i/d_{50})\tau_{b,\text{cr},d50}]$ = dimensionless bed-shear stress parameter of fraction i ,
 $\tau_{b,\text{cr},d50}$ = critical bed-shear stress of sand based on d_{50} ,
 $\tau_b = \mu_c\tau_{b,c} + \mu_w\tau_{b,w}$ = effective bed-shear stress due to current and waves, $s=\rho_s/\rho$ = relative density,
 $\chi = (1+p_{\text{gravel}})(1+p_{\text{mud}})^3$ = factor representing effect of mud and gravel on the critical shear stress of sand,
 $\lambda_i = (d_i/d_{50})^{0.25}$ = roughness correction factor of fraction i ,
 $\zeta_i = (d_{50}/d_i)^{0.5}$ = hiding-exposure factor of fraction i (maximum 2 and minimum 0.5),
 v = kinematic viscosity coefficient, ρ_s = sediment density (input value), ρ = fluid density,
 p_{mud} = fraction of mud (<0.062 mm) of top layer of bed (0 to 0.3),
 p_{gravel} = fraction of gravel (> 2 mm) of top layer of bed (0 to 0.1).

The critical bed-shear stress of Shields (with d_{50}) is represented by:

$$\tau_{b,cr} = (\rho_s - \rho) g d_{50} [0.3/D_* + 0.055(1 - e^{-0.02D_*})] \quad (12)$$

The bed-shear stresses at time t due to currents and waves are represented as:

$$\tau_{b,c} = \rho (u_{*,c})^2 \text{ with } u_{*,c} = \kappa u_z / \ln(30z/k_{s,c}) \quad (13)$$

$$\tau_{b,w} = 0.25 \rho f_w (U_w)^2 \quad (14)$$

with: $\kappa = 0.4$ and $u_z =$ flow velocity at $z \cong 0.1 h$, $U_w = (2\pi/T_p)A_w =$ peak orbital velocity (linear wave theory), $A_w =$ peak orbital excursion, $T_p =$ peak wave period, $f_w = \exp(-6 + 5.2(A_w/k_{s,w})) =$ wave-related friction coefficient, $\rho =$ fluid density including salinity effect; $k_{s,c} =$ current-related roughness, $k_{s,w} =$ wave-related roughness.

The effective bed-shear stresses at time t for sediment transport are represented as:

$$\tau_{b,c}' = \mu_c \tau_{b,c} \quad (15)$$

$$\tau_{b,w}' = \mu_w \tau_{b,w} \quad (16)$$

$\mu_c = f_c'/f_c =$ current-related efficiency factor, $f_c = 0.24/(\log(12h/k_{s,c}))^2 =$ current-related friction coefficient, $f_c' = 0.24/(\log(12h/d_{90}))^2 =$ grain-related friction coefficient, $d_{90} =$ grain size, $\mu_w = 0.7/D_* =$ wave-related efficiency factor ($\mu_{w,min} = 0.14$, $\mu_{w,max} = 0.35$).

The suspension number ZS of sand is represented as:

$$\text{SF: } ZS = w_{sand,o}/(\beta \kappa u_{*,cw}) + 2.5(w_{sand,o}/u_{*,cw})^{0.8} (c_{a,sand}/c_o)^{0.4} + (\rho_{sa}/\rho_{fresh} - 1)^{0.4} \quad (17a)$$

$$\text{MF: } ZS_i = w_{sand,i,o}/(\kappa u_{*,cw}) + 2.5(w_{sand,o}/u_{*,cw})^{0.8} (c_{a,sand}/c_o)^{0.4} + (\rho_{sa}/\rho_{fresh} - 1)^{0.4} \quad (17b)$$

with: $w_{sand,o} =$ fall velocity of single sand particle based on d_{50} , $w_{sand,i,o} =$ fall velocity of fraction i , $\kappa = 0.4$, $\beta = 1 + 2(w_{sand,o}/u_{*,cw})^2 =$ coefficient ($\beta_{max} = 1.5$), $u_{*,cw} = (u_{*,c}^2 + u_{*,w}^2)^{0.5} =$ bed-shear velocity due to current and waves, $u_{*,c} = (\tau_{b,c}/\rho)^{0.5} =$ current-related bed-shear stress, $u_{*,w} = (\tau_{b,w}/\rho)^{0.5} =$ wave-related bed-shear stress, $c_{a,sand} =$ total reference concentration, $c_o = 0.65 =$ maximum bed concentration, $\rho =$ fluid density including salinity effects, $\rho_{fresh} =$ fluid density of fresh water ($= 1000 \text{ kg/m}^3$).

Equation (17) represents the effects of downward gravity settling, upward turbulence mixing (first term), damping due to vertical sediment concentration gradients (second term) and damping due to vertical salinity gradients (third term), (Winterwerp 2001; Van Rijn 1984, 1993, 2007). The damping due to vertical salinity/density gradients mainly occurs during the flood period when the salt wedge penetrates landward. A larger ZS-value yields smaller concentrations.

The time lag effect of the suspended sand concentrations and suspended transport rate can be computed by applying an exponential adjustment of the reference concentration at time t based on: $dc_a/dt = -A(c_{a,t} - c_{a,t,eq})$, resulting in (Van Rijn, 2015):

$$c_{a,sand,t} = c_{a,sand,t-\Delta t} + dc_{a,sand} \quad (18)$$

$$c_{a,sand,t} = [1/(1 + A \Delta t)] [c_{a,sand,t-\Delta t} + A \Delta t c_{a,sand,eq,t}]$$

with: Δt = time step (5 min), $c_{a,sand,t-\Delta t}$ = suspended reference concentration at previous time ($\sum c_{a,i}$ for multi-fraction method), $c_{a,sand,eq,t}$ = equilibrium reference concentration at time t,
 $A = \gamma_c 0.05 (1/h) (w_{sand,o}/u_{*,cw}) (1 + 2w_{sand,o}/u_{*,cw}) (1 + H_s/h)^2$, $A_{minimum} = 0.0005$,
 γ_c = calibration coefficient (range 0.5 to 2; default =1).

The suspended sand transport q_s can be computed by integration of the product of velocity and concentration over the water depth:

$$\text{SF: } q_s = \int_a^h (u c_{sand}) dz \quad \text{with } h = \text{water depth (summation over depth)} \quad (19a)$$

$$\text{MF: } q_s = \sum_o^N \int_a^h (u c_{sand}) dz \quad \text{with } N = 6 = \text{number of fractions (summation over fractions and depth)} \quad (19b)$$

The bed load transport (in kg/m/s) is computed by using a simplified expression (Van Rijn, 2007).

The total load transport of sand at each time t is computed as: $q_{tot} = q_s + q_b$

The tide-integrated sand transport rates are computed by integration over the tidal cycle.

B Wave transformation matrix

The wave transformation matrix transforms measured offshore wave time series from the IJmuiden, Europlatform, Eierlandse Gat and Schiermonnikoog North waverider stations to an arbitrary location nearshore. The wave transformation matrix covers the entire Dutch coast.

The wave transformation matrix uses the following parameters:

- g) wave height (H_{m0}),
- h) mean period (T_{m02}),
- i) wave direction (nautical coordinates),
- j) wind speed,
- k) wind direction
- l) surge

The following steps have been taken to generate the wave transformation matrix:

- 1) Analyse measured data to determine possible combination of wave conditions (wave classification matrices)
- 2) Smooth and bin the wave classification matrices
- 3) Force a SWAN model in stationary mode with the composed set of existing wave conditions
- 4) Generate wave transformation matrix from the results of the SWAN simulations and the observed wave conditions offshore
- 5) Generate input data for the wave stations from a combination of DONAR data (<http://live.waterbase.nl>) and MATROOS data (<http://matroos.deltares.nl>) for timeseries of [H_{m0} , H_{dir} , T_{m02}] until present.
- 6) Validate the transformation matrices with wave observations closer to the shore Lichteiland Goeree, Meetpost Noordwijk and Petten
- 7) Interpolate the SWAN results to refine the transformation matrix
- 8) Make the transformation tool online available in the Deltares repository

The matrix consists of factors specifying the relation between the offshore and nearshore wave parameter. For the significant wave height and peak period for example, the matrix is filled with multiplication factors. An additional factor is used for the wave direction and surge. The output of the wave transformation matrix has been validated with observations at Meetpost Noordwijk (MNP) and a wave buoy near the Amelanders Zeegat (AZB12).

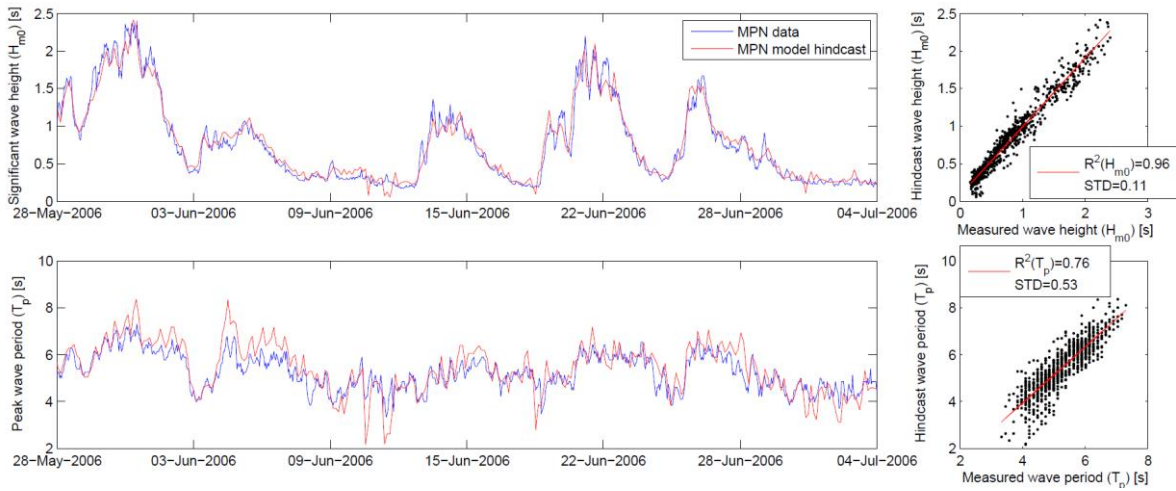


Figure 0.1. Observed wave height and wave period and hindcast from wave transformation matrix for Meetpost Noordwijk (MPN)

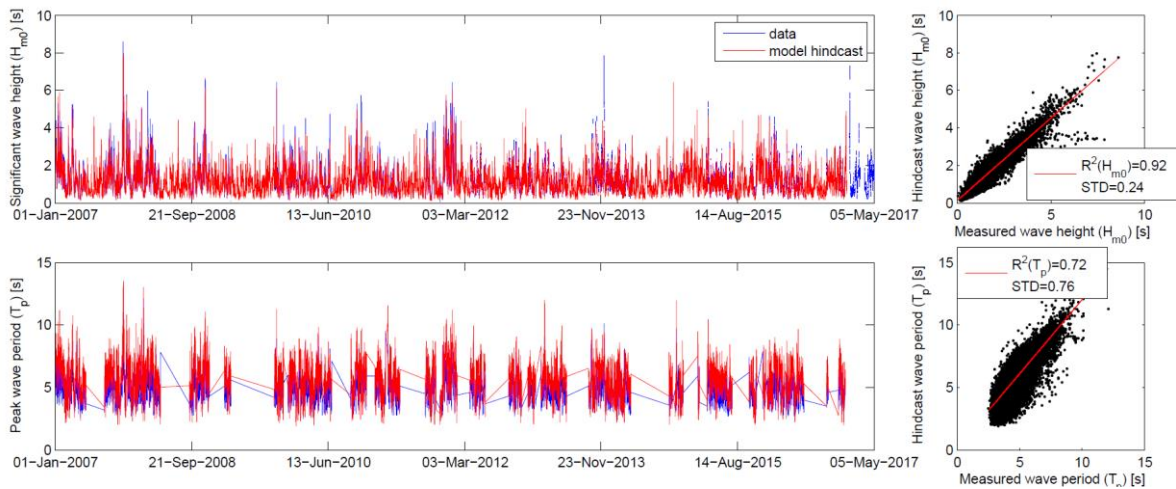


Figure 0.2. Observed wave height and wave period and hindcast from wave transformation matrix for wave buoy near Amelander Zeegat (AZB12)

C Wave time series for NOORDWK20

The wave time series presented here have been obtained using the wave transformation matrix

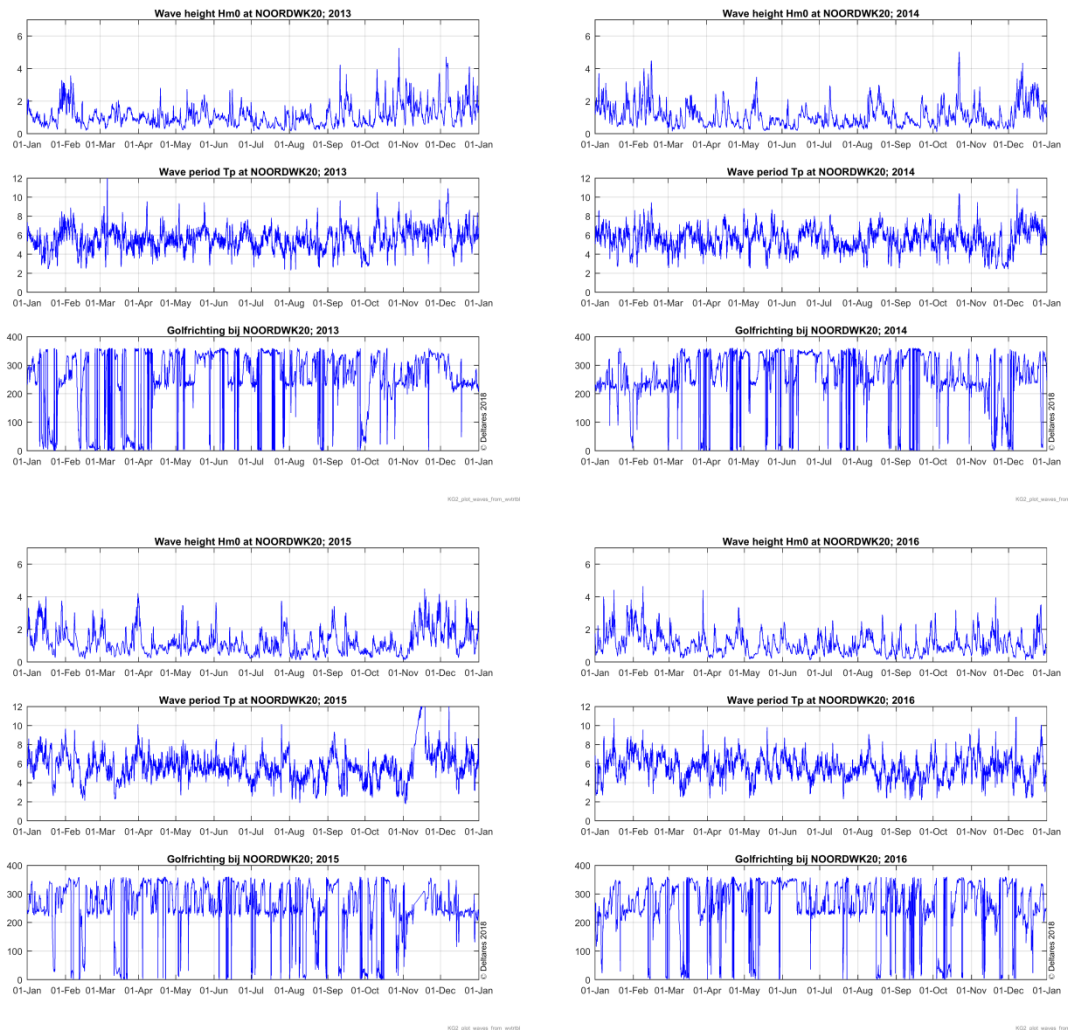


Figure 0.3. Wave height, wave period and wave direction from wave transformation matrix at NOORDWK20 in 2013, 2014, 2015 and 2016

D Joint occurrence tables wave height and direction for NOORDWK20

